

# Overlayers on Silver Nanotriangles: Field Confinement and Spectral Position of Localized Surface Plasmon Resonances

W. Andrew Murray,\* James. R. Suckling, and William L. Barnes

*School of Physics, University of Exeter, Exeter, EX4 4QL, U.K.*

*Received April 10, 2006; Revised Manuscript Received May 25, 2006*

## ABSTRACT

We studied the spectral evolution of plasmon modes associated with silver nanotriangles as a function of dielectric overlayer thickness in the range of 5–300 nm. A substantial red-shift of the resonance is observed that oscillates with increasing over-layer thickness. We explain this previously unreported oscillation through the cavity quantum electrodynamical effect of the array of triangles combined with the dielectric overlayer. The red-shift, though substantial, is less than expected. Comparison with numerical models indicates that this discrepancy is due to very tight field confinement around the tips of the triangles.

Particles that are small compared to the wavelength of light, but large enough to be described by the bulk relative permittivity of the constituent material, exhibit anomalous optical properties. In contrast to the discrete electron excitations in molecules, it is the collective response of the electrons contained within the particle that determines the overall optical characteristics. The amount of light absorbed and re-radiated (scattered) depends sensitively on the composition, size, and shape of the particle as well as the composition of the embedding medium.<sup>1</sup> For particles formed from noble metals, the optical response is determined by the delocalized free-electron charge density and results in resonant scattering and absorption (collectively referred to as extinction) within the visible spectrum. These resonant oscillations of the free electrons are referred to as localized surface plasmon resonances (LSPR)<sup>2</sup> and lead to a locally enhanced electromagnetic field relative to the incident field, an enhancement that is exploited in fields such as surface-enhanced Raman scattering (SERS),<sup>3–5</sup> near-field microscopy,<sup>6</sup> surface-enhanced fluorescence,<sup>7,8</sup> and molecular sensing.<sup>9</sup>

In this study, particles were fabricated on a glass substrate. If the particles so formed are coated with a thin dielectric layer, the field distribution associated with the LSPR is altered; the most important effect being a change (reduction) in the resonant frequency. Initially, as the thickness of the layer coating the particles is increased more of the particles' electromagnetic field samples the material and the resonant frequency is reduced still further. For a thickness greater than

the decay length of the LSPR, the field is contained almost entirely within the coating material and the shift in position of the resonance approaches an asymptotic value. This has been observed by Haes et al. who monitored the resonance position as successive layers of a self-assembled monolayer (SAM, refractive index  $n \approx 1.5–1.6$ ) were attached to Ag and Au particles formed by nanosphere lithography.<sup>10</sup> The average thickness of each successive dielectric layer in the study by Haes et al. was 1.4 nm for the Au particles and 1.6 nm for the Ag particles. Normal incidence extinction spectra were recorded after each layer was added, and the position of the dipolar-type extinction peak ( $\lambda_{\max}$ ) was monitored. The maximum thickness was  $\sim 30$  nm, corresponding to upward of 20 self-assembled monolayers. The peak position,  $\lambda_{\max}$ , was observed to red-shift and approach saturation for a relative shift  $\Delta\lambda_{\max} \approx 120$  nm. More recently, similar types of arrays were coated with monomolecular layers of aluminum oxide allowing a much higher resolution in the layer thickness.<sup>11</sup> A comparable maximum relative shift was observed taking into account the differing refractive indices of the coating materials used in each study. For sensing applications, it is important that the resonant frequency be as sensitive as possible to a change in the external environment. Enoch et al. have shown that closely spaced particle pairs have a greater sensitivity than individual particles.<sup>12</sup> Also, particle aspect ratio and shape is important with triangular particles exhibiting an increased sensitivity over disk-shaped particles and an increasing aspect ratio (major axis divided by minor axis), resulting in an increased sensitivity.<sup>10</sup> Other investigations have focused on the LSPR

\* Corresponding author. E-mail: w.a.murray@ex.ac.uk.

response to the adsorption of single layers of SAM molecules with varying chain length,<sup>13</sup> how changing particle size, shape, and composition alters the near-field sensitivity of the LSPR,<sup>14,15</sup> and the effect of immersing substrate supported nanoparticles in bulk solvents.<sup>15–17</sup> These studies may be separated into two groups; those relating to layers of material with a thickness much smaller and those for layers much thicker than the wavelength of the incident radiation. A third scenario is that relating to particles located on or within layered media with a thickness of the order of the wavelength of the incident radiation. This too can lead to changes in the way light is absorbed and scattered by the particles. Linden et al.<sup>18,19</sup> demonstrated that the LSPR of gold nanoparticles arranged in a periodic array on the surface of an asymmetric waveguide is significantly altered if the frequency of the resonance coincides with that of a waveguide mode. By changing the periodicity of the nanoparticle array, they were able to sweep the frequency of the waveguide modes through the LSPR. They observed a suppression of the extinction associated with the LSPR when the modes overlapped and concluded that this was a consequence of destructive interference between electromagnetic fields associated with the incident light and the waveguide modes. Holland and Hall found that the resonant frequency of the LSPR underwent a shift even in the absence of waveguide modes.<sup>20</sup> A silver island film was thermally deposited onto a lithium fluoride spacer layer coating a continuous silver film. By varying the thickness of the spacer layer, they were able to monitor the spectral form of the LSPR as a function of separation from the silver mirror. Initially, a red-shift of the resonance was observed compared to the value in the absence of the silver mirror, gradually becoming a blue-shift upon increasing the spacer layer thickness.

Modifying the behavior of oscillating charge densities has been well documented in particular when molecular dipole emitters are placed within confined geometries.<sup>21–23</sup> As with particle resonances, the electronic excitations in atomic and molecular entities located near interfaces are different from those located in a bulk, optically isotropic medium. This occurs by changing the boundary conditions of the electromagnetic field in the vicinity of the moiety (for instance, by introducing a planar surface). This well-established concept is the basis behind the field of cavity quantum electrodynamics.<sup>24</sup> The experiments by Drexhage (summarized in ref 21) on the molecular emission from europium ( $\text{Eu}^{3+}$ ) chelate molecules illustrated an oscillatory dependence of the lifetime (inverse decay rate) with separation from a planar metallic–dielectric interface. A similar dependence was found for molecules located near an interface bounded by dielectrics of differing refractive indices. In both systems, the observations could be explained using a model developed by Chance, Prock, and Silbey (CPS theory)<sup>25</sup> that treats the emitters as forced, damped dipole oscillators. This classical approach accounts for the presence of an interface by allowing the driving field to be represented by the retarded dipole field reflected from the interface. The phase relationship between the instantaneous and retarded fields is the key to understanding the oscillatory dependence of the lifetime. If the

fields are in phase, then the total driving field is enhanced; and if the fields are out of phase, then the total driving field is inhibited. The optical path length, governed by the distance of the oscillator from the interface, is therefore crucial in determining the resonant behavior.

For particles much smaller in size than the wavelength of the incident radiation, the LSPR may be approximated as a dipole resonator.<sup>1,2</sup> By analogy with the optical properties of light-emissive molecules, if a small particle is located within a finite geometry then the local photonic density of states may be modified. The field driving the oscillation of the conduction electrons is reduced or enhanced depending on the relative phase of the dipole field and reflected fields. This was identified by Holland and Hall as the cause of the frequency variation in their experiments<sup>20</sup> as CPS theory predicts a fluctuation in the resonant frequency as well as the lifetime of the oscillator. It is most convenient and practical for one to monitor the lifetime of the molecules when studying molecular emitters because usually only a very small perturbation of the resonant frequency is expected due to the small oscillation strength of the optical transitions. This changes for resonant particle oscillations, and a measurable frequency shift occurs owing to the much higher effective oscillator strength of these resonances, as shown by Holland and Hall.<sup>20</sup> In this paper, we present the transmittance spectra obtained from arrays of supported Ag nanoparticles coated with dielectric layers of varying thickness. The resonant frequency of the LSPR is determined as a function of thickness of the overlying dielectric layer from transmittance and extinction measurements. The shift in frequency is modeled using a classical dipole description of the resonant mode associated with the particle embedded in a multilayer structure. A finite element analysis of the structures is also employed to allow conclusions to be drawn as to the effect of the electromagnetic fields within confined structures on the LSPR.

The Ag nanoparticles were fabricated using NSL as described previously.<sup>26</sup> A fused silica substrate ( $25 \times 25 \times 1 \text{ mm}^3$ ) was cleaned in a piranha solution (3:1  $\text{H}_2\text{SO}_4$ /30%  $\text{H}_2\text{O}_2$ ) for 2 h. This was followed by a rinse in ultrapure water and sonication in 5:1:1  $\text{NH}_4\text{OH}$ /30%  $\text{H}_2\text{O}_2$ /H<sub>2</sub>O for 1 h. The final stage of substrate preparation was another rinse in ultrapure water in which the substrates were stored until use. Polystyrene spheres with a mean diameter of 390 nm were supplied in monodispersed solutions (Duke Scientific). After dilution with ultrapure water, the solution was dropped onto the hydrophilic substrate and dispersed across the surface by a gentle rotation and tipping motion. As the water evaporates, the nanospheres self-assemble into a hexagonally close-packed monolayer array with a periodicity  $\lambda_G \approx 338$  nm. The final stage of the process was to thermally evaporate Ag (99.999% purity, GMBH) through the gaps between the close-packed nanospheres. Subsequent nanosphere removal by ultrasonication in toluene left an array of triangular silver nanoparticles (inset Figure 1a). The width of the nanoparticles measured along the perpendicular bisector was  $\sim 90$  nm. The height is taken to be the value as measured by a quartz crystal thickness monitor during the Ag evaporation

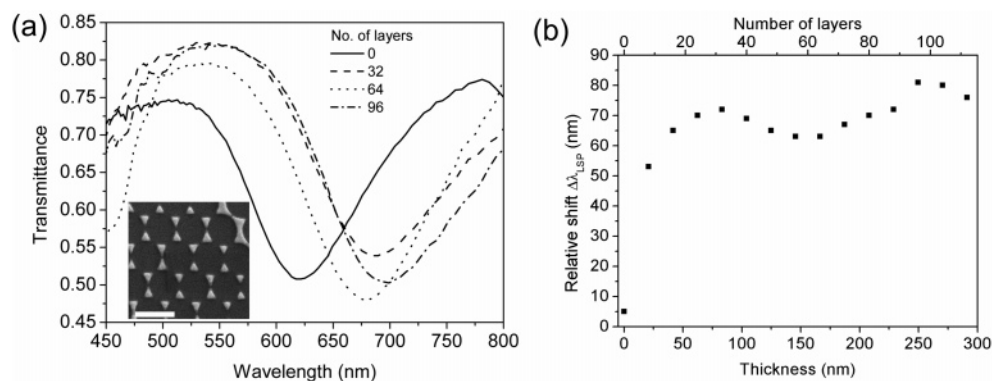


**Figure 1.** Transmittance spectra from sample 1 (particle height = 50 nm) with 0, 32, 64, and 96 overlayers of 22-tricosenoic acid (a) and relative shift of the LSPR plotted as a function of overlayer thickness and number of layers (b). The inset is an SEM image of an uncoated array, scale bar = 500 nm.

process. Two separate samples were fabricated with particle heights of 30 and 50 nm covering an area  $>3 \text{ cm}^2$  on each substrate.

To deposit a known thickness of an optically transparent dielectric, we used the Langmuir–Blodgett<sup>27</sup> (LB) technique, as described elsewhere.<sup>22</sup> A stepped overlayer structure was built up on each sample by the sequential deposition of an amphiphilic molecule, 22-tricosenoic acid. To form a monolayer, the molecule is dispersed in chloroform and the solution is spread onto a water sub-phase. The disordered layer of molecules at the surface is then compressed to a surface pressure of  $30 \text{ mNm}^{-1}$ . At this pressure, the molecules align perpendicular to the surface of the water with the hydrophobic alkyl chain pointing vertically upward and the hydrophilic carboxyl headgroup immersed in the water. Deposition of the layer onto the particle array proceeds by dipping the sample vertically at a downstroke rate of  $0.25 \text{ mm/s}$  into the sub-phase, collecting the aligned monomolecular layer on the way. To obtain a uniform deposition, the surface pressure was maintained by continually compressing the film during dipping. A second monomolecular layer was deposited on top of the first as the sample was drawn out of the sub-phase (upstroke rate =  $0.20 \text{ mm/s}$ ). This yields a combined bilayer thickness of  $5.2 \text{ nm}$  and was the best spatial resolution the technique could afford for samples prepared in this study. The sample consisting of  $50\text{-nm}$ -high particles is referred to as sample 1 for the remainder of this article and was prepared with 15 regions each with a different thickness of 22-tricosenoic acid in a  $3 \times 5$  array. The thickness ranged from 0 layers to 112 layers ( $\sim 291 \text{ nm}$ ) in 8-layer ( $\sim 21 \text{ nm}$ ) steps. The sample consisting of  $30\text{-nm}$ -high particles is referred to as sample 2 and was similarly prepared with 16 regions in a  $4 \times 4$  array allowing a maximum thickness of 120 layers ( $\sim 312 \text{ nm}$ ).

Normal incidence transmittance spectra were taken from each of the regions before and after depositing the  $\omega$ -tricosenoic acid. A collimated beam with a divergence of  $\sim 0.5^\circ$  and diameter of  $\sim 1 \text{ mm}$  obtained from a tungsten halogen lamp was directed onto the samples. A monochromator was used to spectrally filter the incident light (spectral width  $\sim 2 \text{ nm}$ ), while a mechanical chopper modulated the intensity of the incident light to allow phase-sensitive detection of

the zero-order transmitted and reflected beams. Furthermore, a beam splitter redirected a small fraction of the incident beam onto a second detector to allow source fluctuations to be taken into account.

The data shown in Figure 1a illustrates the evolution of the LSPR as progressively thicker overlayers are deposited on four regions of sample 1. Normal incidence transmittance spectra of the coated nanoparticle arrays generally showed two main features. First a transmittance minimum is observed at wavelengths between  $620$  and  $700 \text{ nm}$ , the particular wavelength depending on the overlayer thickness. This is indicative of the dipolar-type LSPR. Without any 22-tricosenoic acid overlayers deposited, the LSPR minimum is located at  $620 \text{ nm}$ . With 32 layers ( $83 \text{ nm}$ ) deposited, the resonance is seen to red-shift to a value of  $690 \text{ nm}$ ; at the same time, it also broadens and becomes shallower. Increasing the total thickness to 64 layers ( $166 \text{ nm}$ ), the resonance position blue-shifts to a value of  $675 \text{ nm}$  and appears to deepen and narrow. With 96 layers ( $250 \text{ nm}$ ) deposited, the position again red-shifts to a slightly higher value of  $698 \text{ nm}$ , broadens, and shallows. Second, a drop in transmittance is observed at wavelengths below  $470 \text{ nm}$  that becomes most pronounced for an overlayer thickness of 64 layers. This may be attributed to a combination of effects, primarily the appearance of a quadrupolar-type resonant mode of the particle.<sup>28</sup> Without any overlayer deposited, this quadrupolar mode is beyond the spectral range of the experimental setup (less than  $450 \text{ nm}$ ); however, as LB layers are deposited the mode is red-shifted so that the longer wavelength wing of the resonance is observed in the transmittance data. Figure 1b is a plot of the position of the minimum in the transmittance spectra associated with the dipolar resonance. After an initial steep rise, there is a clear oscillation in the data with maxima at  $\sim 32$  layers and  $\sim 96$  layers and a minimum between 58 and 62 layers.

In Figure 2a, transmittance spectra are shown from sample 2 (silver now  $30 \text{ nm}$  thick rather than  $50 \text{ nm}$  thick). With no overlayer deposited, the position of the LSPR is at a higher wavelength compared to sample 1 as has been well documented.<sup>29</sup> An approximately linear red-shift is observed with decreasing particle height in this size regime. The response to the addition of overlayers on sample 2 is observed from

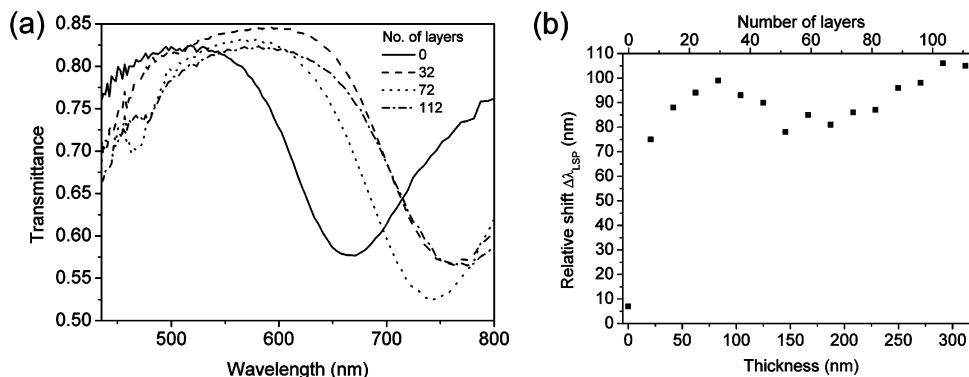


**Figure 2.** Transmittance spectra from sample 2 (particle height = 30 nm) with 0, 32, 64, and 96 overlayers of 22-tricosenoic acid (a) and relative shift of the LSPR plotted as a function of overlayer thickness and number of layers (b).

transmittance spectra to be similar in character to sample 1, an initial red-shift with the addition of 32 layers followed by a blue-shift with 72 layers deposited and a further red-shift with 112 layers deposited. The relative size of the shift (plotted in Figure 2b as a function of dielectric thickness) is larger than that observed for sample 1, similar to the effect reported by Haes et al. from arrays formed using NSL coated with self-assembled monolayers.<sup>10</sup>

To gain a better understanding of the frequency shifts and behavior of the dipolar LSPR described above, we used the CPS model for a classical dipole oscillator.<sup>25</sup> This has been applied extensively in describing the behavior of forced, damped electric dipole emitters embedded in multilayered planar structures. Because the LSPR monitored in the experimental work detailed above is the dipolar-type resonance, at face value CPS theory should lend itself well to representing the system. However, there are significant differences, mainly in the fact that a single point dipole is modeled, thus neglecting the effects of neighboring dipoles. Moreover, CPS theory is designed to be implemented with planar structures. In our samples, the particles protrude from the surface so that the LB overlayers subsequently deposited onto the particles have a similar profile, particularly when the number of layers  $N < 20$ . Although CPS theory does not allow an exact representation of the system analyzed experimentally, some insight can be obtained by approximating the system as consisting of four planar layers, illustrated in the inset of Figure 3. The top layer and bottom layer are the semi-infinite air and silica regions, respectively; the upper-middle layer is the LB layer. In the model, the particles are represented by locating point dipoles 10 nm above a fourth layer with relative permittivity determined using Maxwell Garnett theory.<sup>1,30</sup> This is the lower-middle layer and is a composite LB/particle layer with a thickness of 50 nm, equal to the height of the particles. By representing the system in this way, the general response to an electromagnetic field is governed by the relative permittivities of the layers with the dipoles inserted to act as both source and probe of those fields.

Maxwell Garnett theory treats a composite layer with particulate inclusions in an otherwise homogeneous embedding medium as having an average relative permittivity  $\epsilon_{av}$

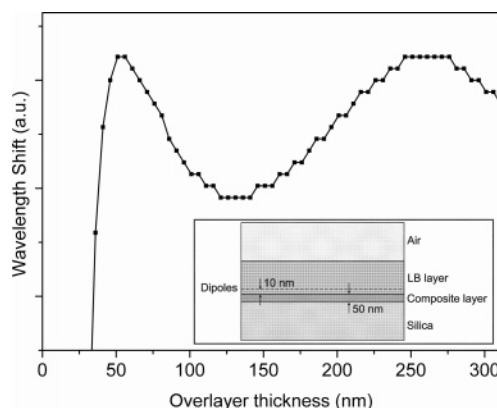


**Figure 3.** Theoretical plot of the wavelength shift (arbitrary units) as a function of overlayer thickness of a dipole oscillator located within the layered structure as shown (inset).

$$\epsilon_{av} = \frac{(1-f)\epsilon_d + f\lambda_k\epsilon_m}{1-f + f\lambda_k} \quad (1)$$

where  $\epsilon_d$  is the relative permittivity of the inclusions,  $\epsilon_m$  is the relative permittivity of the embedding medium, and  $\lambda_k$  is a tensor with principal components

$$\lambda_k = \frac{\epsilon_d}{\epsilon_d + L_k(\epsilon_m - \epsilon_d)} \quad (k = 1, 2, 3) \quad (2)$$

where  $L_k$  is one of the three geometrical factors associated with the three principal axes of an oblate spheroid.<sup>1</sup> Because the light is normally incident and is polarized parallel to the substrate (and therefore parallel to the long axis of the particle), only one component of  $\lambda_k$  is required. To calculate a value for  $\epsilon_{av}$ , all that remains is to define suitable values for the filling fraction  $f$  and geometrical factor  $L_k$ . The geometrical factor  $L_k$  is chosen to produce a particle resonance at  $\lambda_{max} = 680$  nm, the approximate position of the resonance with a thick LB overlayer deposited onto the particle. At this wavelength, the relative permittivity of silver was taken to be  $\epsilon_m = -19.0 + 1.2i$ .<sup>31</sup> The relative permittivity of the 22-tricosenoic acid is known to be anisotropic with a value perpendicular to the molecular axis (parallel to the substrate) of  $\epsilon_d = 2.49$ .<sup>32</sup> A resonance occurs

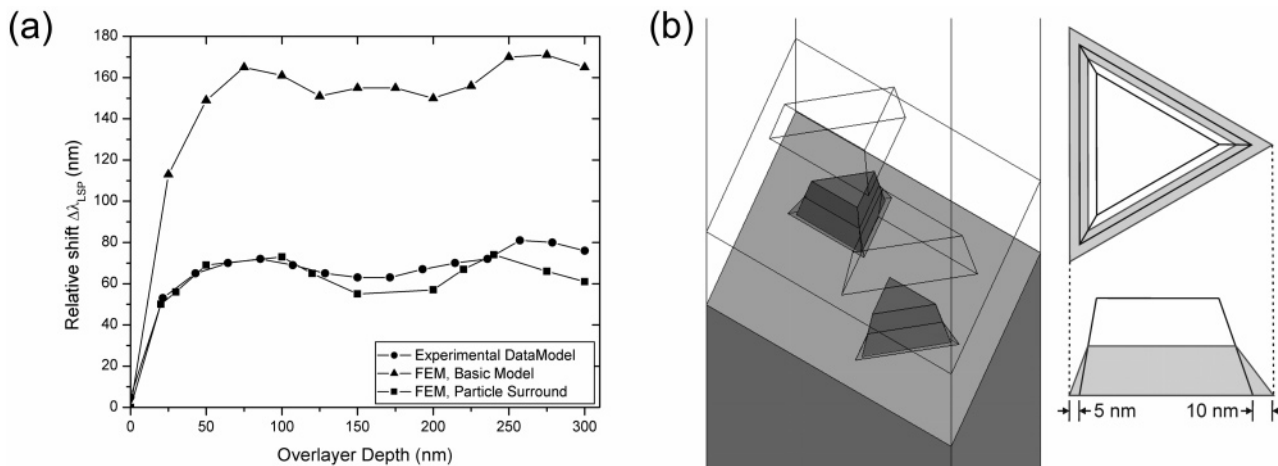


**Figure 4.** (a) Relative shift of the LSPR as a function of overlayer thickness obtained from finite element models of sample 1; circles are the experimental data, and triangles are from a basic model in which the particles were represented as vertical-sided prisms. Squares are from the final model illustrated in b showing the repeat unit cell of the coated nanoparticles surrounded by a cavity region about the base. Also included is a plan and side view of a single nanoparticle; the shaded region represents the cavity with the baseline running parallel to and separated by 5 nm from the baseline of the particle.

when the denominator of eq 2 is minimized, this occurring when  $L_k = 0.12$  upon insertion of the silver and 22-tricosenoic acid relative permittivities. These values are substituted into eq 1 with  $f = 0.1$ , chosen to provide an approximate match to that of the nanoparticle array studied in the experiment.

Incorporating these parameters into the multilayer CPS theory results in the theoretical plot of the shift in wavelength (for ease of comparison with the experimental data) as a function of overlayer thickness,  $d$ , shown in Figure 3. Up to a thickness of 20 layers, a steep rise is observed in the magnitude of the frequency shift. As the thickness increases further, the shift begins to level off, indicating that the near field associated with the dipole that extends into the overlayer has decayed sufficiently so as not to extend into the semi-infinite air layer. Thereafter, an oscillation is observed in the data with a minimum at 150 nm and a maximum at 250 nm. As referred to above, this is due to the phase relationship between the emitted dipole field and the multiply reflected dipole field within the LB layer. Comparing the theoretical plot with the experimental data of Figure 1b, there is reasonable agreement in the positions of the maxima and minima, although the strength of the different features are not well accounted for. It is noted that the amplitude of the oscillation is very much smaller than that observed experimentally. Given that the model is different in many ways from the experiment, an exact match with regard to the amplitude would not be expected. However, the overriding parameter in determining the position of the peaks and troughs is the optical path length of the reflected field. This would be consistent in both the theory and experiment. Furthermore, changes to the spectral form of the LSPR could be explained using a related argument. The position and width of the resonance is determined partly by the radiative damping experienced by the collective electron oscillation. If the photonic mode density near the dipole is reduced, then this radiative energy loss route is inhibited, as would occur if the phase of the reflected dipole field does not match that

of the dipole itself. A reduction in radiative damping is accompanied by a blue-shift and narrowing of the resonance,<sup>2</sup> as observed in the experimental data presented here.

To consolidate this explanation of the origin of the frequency shift, the structures were also modeled using a commercially available finite element (FE) modeling package (high-frequency structure simulator (HFSS), Ansoft Corporation, Pittsburgh, PA). Using this method, the nanoparticles and surrounding environment are constructed from a number of tetrahedrons. Maxwell's equations are then used to match the electromagnetic fields across the boundaries of the tetrahedrons, thus allowing the response of the structure to an incident electromagnetic field to be modeled. Initially, a simple model was constructed consisting of vertically sided prism-shaped silver particles supported by a silica substrate. The dielectric over-layer was designed such that it followed the contours of the particle/substrate surface to any specified depth. This resulted in a resonant wavelength shift with an over-layer depth that was too large when compared to the experimental data;  $\sim 160$  nm as opposed to  $\sim 70$  nm, as shown in Figure 4a. To obtain better agreement, the shape of the particle was altered from prism-shaped to that of a truncated tetrahedron. This concentrates the electromagnetic field enhancement at the tips of the particle around the particle base. Without other amendments to the model, it was found that this did little to enhance the fit of the modeled optical response to the experimental data. However, the fit was improved greatly by creating a cavity region around the base of the particle described by a reduced relative permittivity ( $\epsilon_d = 1.2$ ) such as would occur if the initial overlayer did not contact the surface entirely.

There are several assumptions built in to the parameters we have used here. As noted above, we have ignored the anisotropy of the LB film, and we have also ignored the changing orientation of the LB film in the first few monolayers.<sup>33</sup> These assumptions have been found to be applicable before in studies of this type.<sup>22</sup> For the cavity region, we sought to use a relative permittivity between that

of air and water, water being a common contaminant of such metallic nanoparticles. Although there were a range of cavity size/relative permittivity combinations that could be used, those reported here gave the best match to the experimental data. A unit cell of the final model is depicted in Figure 4b, where silver particles are shown as dark gray triangles on the lighter substrate, the cavity is seen around the base of the particles, and the overlayer is shown as the wire frame above the substrate. The accompanying diagrams of a single particle illustrate the small dimensions of the cavity (thickness < 5 nm). This combined with the strong effect of its presence on the magnitude of the wavelength shift demonstrate the high confinement of the electromagnetic field associated with the LSPR near the surface of the nanoparticle. A final observation is that the FE model reproduces the oscillation in the resonant shift, as demonstrated in the experimental data.

We have presented experimental results that show how the position of the LSPR varies as a function of the thickness of a dielectric overlayer deposited onto substrate-supported silver nanoparticles formed by nanosphere lithography. Initially, a smooth increase is seen in the resonant wavelength of the LSPR, approaching a saturated value in line with previous studies.<sup>10</sup> When the thickness of the overlayer is increased beyond this point, the resonant wavelength was still observed to depend sensitively on the thickness, exhibiting an oscillatory dependence. By comparing the experimental data with the theoretical data produced for a multilayer structure, we identified this behavior as being due to the influence of the field reflected by the LB/air interface on the dipole oscillation. In fact, it is the net field reflected back to the particle (dipole) site that is important. One can view this process as the response of any individual nanoparticle being modified by the reflections of the other particles in the array as seen in the partial mirror of the LB/air interface. Further confirmation of this behavior was supplied by using a finite element model to determine the electromagnetic response of the structures. This also indicated an oscillation in the LSPR frequency beyond the expected saturation point. In addition, to obtain reasonable agreement between theory and data, we incorporated into the model a small region partially filled with dielectric surrounding the base of the particle. This dramatically reduced the overall shift predicted by the model, illustrating the tight confinement of the electromagnetic field near the particle.

We suggest that this work may find relevance in the design and optimization of photonic devices, in particular particle-plasmon-based sensing applications. By locating the particles within confined geometries, it is possible for one to both suppress and enhance the coupling of light into the LSPR and to shift the resonance. Similarly, the reverse process whereby the LSPR undergoes radiative decay may also be altered. We therefore suggest that the fluorescence enhancement exhibited by molecules that couple to the LSPR field may be further influenced by their incorporation into layered structures.

**Acknowledgment.** We thank the Engineering and Physical Sciences Research Council (EPSRC) for financial sup-

port. We further acknowledge valuable discussions with Tomas Rindzevicius and Mikael Kall, both of Chalmers University, and with Richard P. van Duyne and George C. Schatz, both of Northwestern University. This work was also supported by the EU project “Surface Plasmon Photonics”, NMP-CT-2003-505699; the EU Network of Excellence, Phoremot; and the University of Exeter. W.L.B. is a Royal Society Merit award holder.

## References

- (1) Bohren, H. F.; Huffman, D. R. *Absorption and Scattering of Light by Small Particles*; Wiley: New York, 1983.
- (2) Kreibig, U.; Vollmer, M. *Optical Properties of Metal Clusters*; Springer-Verlag: Berlin, 1995.
- (3) Schatz, G. C.; Van Duyne, R. P. In *Handbook of Vibrational Spectroscopy*; Chalmers, J. M., Griffiths, P. R., Eds.; Wiley: Chichester, 2002; pp 759–774.
- (4) Nie, S. M.; Emery, S. R. *Science* **1997**, *275*, 1102–1106.
- (5) Wokaun, A.; Gordon, J. P.; Liao, P. F. *Phys. Rev. Lett.* **1982**, *48*, 957–960.
- (6) Pohl, D. W. In *Near-Field Optics and Surface Plasmon Polaritons*; Kawata S., Ed.; Springer-Verlag: Heidelberg, 2001; Vol. 81, p 1.
- (7) Dittbacher, H.; Felidj, N.; Krenn, J. R.; Lamprecht, B.; Leitner, A.; Aussenegg, F. R. *Appl. Phys. B: Lasers Opt.* **2001**, *73*, 373–377.
- (8) Kulakovich, O.; Strekal, N.; Yaroshevich, A.; Maskevich, S.; Gaponenko, S.; Nabiev, I.; Woggon, U.; Artemyev, M. *Nano Lett.* **2002**, *2*, 1449–1452.
- (9) Okamoto, T.; Yamaguchi, I.; Kobayashi, T. *Opt. Lett.* **2000**, *25*, 372–374.
- (10) Haes, A. J.; Zou, S.; Scahtz, G. C.; Van Duyne, R. P. *J. Phys. Chem. B* **2004**, *108*, 109–116.
- (11) Whitney, A. V.; Elam, J. W.; Zou, S.; Zinovev, A. V.; Stair, P. C.; Schatz, G. C.; Van Duyne, R. P. *J. Phys. Chem. B* **2005**, *109*, 20522–20528.
- (12) Enoch, S.; Quidant, R.; Badenes, G. *Opt. Express* **2004**, *12*, 3422–3427.
- (13) Duval-Malinsky, M.; Kelly, K. L.; Schatz, G. C.; Van Duyne, R. P. *J. Am. Chem. Soc.* **2001**, *123*, 1471–1482.
- (14) Haes, A. J.; Zou, S.; Schatz, G. C.; Van Duyne, R. P. *J. Phys. Chem. B* **2004**, *108*, 6961–6968.
- (15) Mock, J. J.; Smith, D. R.; Schultz, S. *Nano Lett.* **2003**, *3*, 485–491.
- (16) Xu, G.; Tazawa, M.; Jin, P.; Nakao, S.; Yoshimura, K. *Appl. Phys. Lett.* **2003**, *82*, 3811–3813.
- (17) Meriaudeau, F.; Downey, T. R.; Passian, A.; Wig, A.; Ferrell, T. L. *Appl. Opt.* **1998**, *37*, 8030–8037.
- (18) Linden, S.; Kuhl, J.; Giessen, H. *Phys. Rev. Lett.* **2001**, *86*, 4688–4691.
- (19) Linden, S.; Christ, A.; Kuhl, J.; Giessen, H. *Appl. Phys. B: Lasers Opt.* **2001**, *73*, 311–316.
- (20) Holland, W. R.; Hall, D. G. *Phys. Rev. Lett.* **1984**, *52*, 1041–1044.
- (21) Drexhage, K. H. In *Progress in Optics XII*; Wolf, E., Ed.; North-Holland: Amsterdam, 1974; p 165.
- (22) Amos, R. M.; Barnes, W. L. *Phys. Rev. B* **1997**, *55*, 7249–7254.
- (23) Worthing, P. T.; Amos, R. M.; Barnes, W. L. *Phys. Rev. A* **1999**, *59*, 865–872.
- (24) See, for example, *Cavity Quantum Electrodynamics*; Berman, P. R., Ed.; Academic: San Diego, CA, 1994.
- (25) Chance, R. R. *Adv. Chem. Phys.* **1978**, *37*, 1.
- (26) Murray, W. A.; Astilean, S.; Barnes, W. L. *Phys. Rev. B* **2004**, *69*, 165407.
- (27) Blodgett, K.; Langmuir, I. *Phys. Rev.* **1937**, *51*, 964–982.
- (28) Lance-Kelly, K.; Coronado, E.; Zhao, L. L.; Schatz, G. C. *J. Phys. Chem. B* **2003**, *107*, 668–677.
- (29) Jensen, T. R.; Schatz, G. C.; Van Duyne, R. P. *J. Phys. Chem. B* **1999**, *103*, 2394–2401.
- (30) Garnett, J. C. M. *Philos. Trans. R. Soc.* **1904**, *203*, 385–420.
- (31) Palik, E. *Handbook of Optical Constants of Solids*; Academic Press Inc.: London, 1985.
- (32) Barnes, W. L.; Sambles, J. R. *Surf. Sci.* **1986**, *177*, 399–416.
- (33) Barnes, W. L.; Sambles, J. R. *Surf. Phys. Rev. B. Sci.* **1987**, *183*, 189–200.

NL060812E